Enhanced Regeneration of Corneal Tissue Via a Bioengineered Collagen Construct Implanted by a Nondisruptive Surgical Technique

Marina Koulikovska, Mehrdad Rafat, Goran Petrovski, Zoltán Veréb, Saeed Akhtar, Per Fagerholm and Neil Lagali

Original Publication:

Marina Koulikovska, Mehrdad Rafat, Goran Petrovski, Zoltán Veréb, Saeed Akhtar, Per Fagerholm and Neil Lagali, Enhanced Regeneration of Corneal Tissue Via a Bioengineered Collagen Construct Implanted by a Nondisruptive Surgical Technique, 2015, Tissue Engineering. Part A, (21), 5-6, 1116-1130.
http://dx.doi.org/10.1089/ten.tea.2014.0562

Enhanced Regeneration of Corneal Tissue via a Bioengineered Collagen Construct implanted by a Non-disruptive Surgical Technique

Marina Koulikovska MSc[1,2,§], Mehrdad Rafat PhD[2,3,8,§], Goran Petrovski MD PhD[4,5,6], Zoltán Veréb MSc[4,6], Saeed Akhtar PhD[7], Per Fagerholm MD PhD[1,2], and Neil Lagali PhD[1,2*]

[1]Department of Ophthalmology, [2]Institute for Clinical and Experimental Medicine, and [3]Department of Biomedical Engineering, Linköping University, 581 85 Linköping, Sweden
[4]Stem Cells and Eye Research Laboratory, Department of Biochemistry and Molecular Biology and [5]Apoptosis and Genomics Research Group of Hungarian Academy of Sciences, Medical and Health Science Center, University of Debrecen, Debrecen, Hungary
[6]Department of Ophthalmology, University of Szeged, Szeged, Hungary
[7]Department of Optometry, College of Applied Medicine, King Saud University, Saudi Arabia
[8]LinkoCare Life Sciences AB, Mjärdevi Science Park, Teknikringen 10, Plan 3, 583 30 Linköping, Sweden

§ denotes equal contributions
*corresponding author

Short title: Bioengineered constructs for stromal replacement

Keywords: bioengineering, collagen implants, cornea, stem cells, transplantation, regenerative medicine

This work was performed in Linköping, Sweden (biomaterials, surgeries, in vivo study and tissue analysis), Debrecen, Hungary (in vitro stem cell experiments), and Riyadh, Saudi Arabia (TEM imaging).

***Corresponding author:**

Neil Lagali, PhD
Department of Ophthalmology
Institute for Clinical and Experimental Medicine
Linköping University
581 83 Linköping, Sweden
Tel +46 101034658
Fax +46 101033065
Email: neil.lagali@liu.se

Abstract

Severe shortage of donor corneas for transplantation, particularly in developing countries, has prompted the advancement of bioengineered tissue alternatives. Bioengineered corneas that can withstand transplantation while maintaining transparency and compatibility with host cells, and that are additionally amenable to standardized, low-cost mass production, are sought. In this study, a bioengineered porcine construct (BPC) was developed to function as a biodegradable scaffold to promote corneal stromal regeneration by host cells. Using high purity medical-grade type I collagen, high 18% collagen content and optimized EDC-NHS crosslinker ratio, BPCs were fabricated into hydrogel corneal implants with over 90% transparency and fourfold increase in strength and stiffness compared to previous versions. Remarkably, optical transparency was achieved despite the absence of collagen fibril organization at the nanoscale. *In vitro* testing indicated the BPC supported confluent human epithelial and stromal-derived mesenchymal stem cell populations. With a novel femtosecond laser-assisted corneal surgical model in rabbits, cell-free BPCs were implanted *in vivo* in the corneal stroma of 10 rabbits over an 8 week period. *In vivo*, transparency of implanted corneas was maintained throughout the postoperative period, while healing occurred rapidly without inflammation and without the use of postoperative steroids. BPC implants had a 100% retention rate at 8 weeks, when host stromal cells began to migrate into implants. Direct histochemical evidence of stromal tissue regeneration was observed by means of migrated host cells producing new collagen from within the implants. This study indicates that a cost-effective BPC extracellular matrix equivalent can incorporate cells passively to initiate regenerative healing of the corneal stroma, and is compatible with human stem or organ-specific cells for future therapeutic applications as a stromal replacement for treating blinding disorders of the cornea.

Introduction

Corneal blindness is the second largest cause of blindness globally [1], with trauma, disease-related scarring, and ulceration of the cornea responsible for 1.5 to 2 million new cases of blindness per year [2]. Often the only treatment option is surgical transplantation of the cornea, which is limited by the lack of suitable donor tissue, particularly in developing countries [3], where the situation is acute due to significantly higher rates of disease and traumatic eye injury [2]. The problem is also an economic one: in the developing world, facilities for organ donation, harvesting, and storage in eye banks are scarce. Research in recent years has focused on addressing the donor shortage (a problem even in developed nations) by tissue engineering a corneal equivalent. Tissue-engineered biomaterials made from collagen, the principal component of the cornea's extracellular matrix, have in particular shown promise in preclinical [4-7] and clinical [8] studies. These earlier studies demonstrated the ability of the biomaterials to recruit host fibroblasts to interfaces to anchor the implant, and to allow corneal nerves to regenerate within the materials.

The collagen-based materials are designed to function as temporary scaffolds that maintain tissue structure, while the surrounding tissue regenerates and replaces the original scaffold over time [9]. Previous studies, while confirming epithelial cell coverage and innervation of scaffolds, have not definitively demonstrated migration of individual cells into the biomaterial to actively regenerate the stroma, by turnover of implanted collagen into host collagen [4-8]. Whether collagen-based biomaterials are capable of inducing stromal tissue regeneration over time, is unknown.

Recent work, including a human clinical trial [8] has focused on the use of recombinant human collagen to make scaffolds for corneal implantation. Such scaffolds were relatively soft, and resulted in surgical suture-induced ocular surface irregularities that limited vision recovery. It was postulated that stronger scaffolds with increased collagen content and enzymatic resistance, along with modified implantation techniques minimizing suture contact, could solve some of the issues that arose during the human trial [8]. Additionally, recombinant human collagen at present is produced in only a few facilities in very limited quantities, making the material difficult to obtain and expensive for widespread use in corneal tissue-engineering, in particular for applications in developing nations.

Alternatively, efforts by a number of investigators have focused on the use of de-cellularized, chemically-treated pig corneas as an alternative to human donor corneal tissue [10-13]. While this approach has shown promising results in animal models, the standardized procurement, de-cellularization methods, storage procedures, and material certification for human use are lacking and can lead to varying outcomes, for example with respect to transparency of the final constructs [10,13]. Moreover, traces of cytotoxic chemicals used to remove all traces of DNA from the corneas may remain in the constructs [10], the consequences of which are unclear. Additionally, the de-cellularized pig corneas and their properties are fixed and cannot at present be engineered to biodegrade, nor has stem cell compatibility or stromal regeneration after implantation been demonstrated.

Therefore, there remains an urgent need to address issues that arose during previous trials, with a more mature, collagen-based material system that has demonstrated the potential for human use. Here, we report a new bioengineered porcine construct (BPC), based on highly-purified collagen extracted from porcine skin, fabricated with high collagen content (18% by weight) and an optimized cross-linking procedure. The collagen extracted from porcine skin is widely available in medical-grade quality a fraction of the cost of recombinant human collagen. Moreover, skin-sourced collagen is more abundant than recombinant collagen or de-cellularized corneas. High-purity porcine collagen is already used in FDA-approved and CE-marked biomedical devices implanted in humans in non-corneal applications [14, 15] and is therefore a safe and well-characterized raw material. Our earlier studies with tissue-engineered porcine collagen-based corneal implants have shown promising results [6], but such implants had only a fraction of the strength required for optimal human implantation outcomes, and necessitated more invasive surgeries with suturing, which could lead to inflammation and vision-limiting melting and ocular surface unevenness.

In this study we report significantly stronger, yet biodegradable and transparent BPCs designed for human use. Compatibility with human corneal epithelial and mesenchymal stem cells were tested *in vitro*, while cell-free constructs were validated *in vivo* in a new surgical procedure termed femtosecond laser-assisted intra-stromal keratoplasty (FLISK). The surgery minimizes disturbance of the epithelium and maintains corneal shape and curvature without suturing, thereby avoiding stimulation of an aggressive wound healing response. Additionally, FLISK can be considered a therapeutic procedure for replacement of diseased or damaged native stroma, in contrast to micropocket insertion models [10, 12, 13] where native tissue is not excised thus leading to an unnatural refraction and stromal architecture, inflammation, and the need for surgical suturing and use of postoperative steroids. In this study, it was found that the BPC implants maintained the shape and structure of the host cornea while supporting rapid healing and a limited in-growth of host stromal cells, which began to degrade the implanted collagen scaffold and produce new host collagen in less than 8 weeks. The cost-effective raw materials, therapeutic surgical technique, and regenerative potential are expected to provide a range of options in future corneal regenerative studies addressing corneal blindness.

Materials and Methods

Fabrication of bioengineered porcine constructs (BPCs). We have previously reported the basic fabrication process for collagen-based corneal implants [5, 6]. 1-[3-(Dimethylamino)propyl]-3-ethylcarbodiimide methiodide - (EDCM) and N-hydroxysuccinimide (NHS) were purchased from Sigma-Aldrich (St. Louis, USA). Medical grade, high purity porcine Collagen (type-I atelo-collagen) was purchased from SE Eng Co. (Seoul, South Korea). In this study, increased collagen content (18% collagen) was achieved by a controlled vacuum evaporation of a dilute solution (5%) of collagen at room temperature. The novel evaporation technique allowed us to increase the collagen concentration without compromising transparency of the hydrogels. The 18% solution was then crosslinked using the water-soluble cross-linking agents EDCM and NHS. These water soluble cross-

linkers are so-called 'zero-length cross-linkers' that do not become incorporated in the final collagen scaffold [13]. EDCM and NHS were added to the collagen solution at equal molar ratios (1:1:1, EDCM:NHS:collagen), mixed thoroughly and molded in between glass plates to make a homogeneous hydrogel scaffold. A 100 μm thick spacer and a clamping system were used for compression molding of the 100μm thick implants. The same procedure was applied for the 300 μm implants except that a compression molding was not used and the gel was allowed to swell during crosslinking. Samples were then cured at room temperature and then at 37ºC, in 100% humidity chambers. De-molding was achieved by immersion in phosphate buffered saline (PBS) for 1 hour. Samples were subsequently washed four times with PBS solution (1× PBS, containing 1% v/v chloroform) at room temperature to extract out reaction byproducts, and to sanitize the samples.

Evaluation of mechanical and optical properties. The tensile strength, elongation at break (elasticity), elastic modulus (stiffness), and energy at break (toughness) of bioengineered scaffolds were determined using an Instron Series IX Automated Materials Testing System (Model 3343, Instron, Canton, MA) equipped with the BluHill software and a load cell of 50N capacity and pneumatic metal grips at a crosshead speed of 5 mm/min and an initial grip separation of 14 mm. Dumbbell shaped specimens were made by dispensing and curing the collagen-crosslinkers solutions into dumbbell Teflon molds. PBS-equilibrated dumbbell specimens were attached to the grips with a pneumatic pressure of 40 psi and immersed in a temperature-controlled container (BioPuls bath) filled with PBS at 37°C during the test. Light transmission and scatter measurements of BPCs and rabbit corneas were made at room temperature, both for white light (quartz-halogen lamp source) and for narrow spectral regions (centered at 450, 550, and 650 nm) using a custom-built optical instrument [16]. Samples were hydrated in PBS solution before and during the measurement. The light transmission data for healthy human corneas were adopted from the literature.

Evaluation of enzymatic degradation. Collagenase Type I (from Clostridium histolyticum) was used for the Collagenase degradation (resistance) test. Trizma base (Tris base) refers to 2-Amino-2-(hydroxymethyl)-1,3-propanediol and used for preparing Tris-HCl buffer. 50-80 mg of the 100μm thick compression molded hydrogel scaffolds were equilibrated in 5 ml of 0.1M tris-HCl buffer (pH 7.4) containing 5 mM CaCl2 at 37 °C for 1h. Subsequently, 1 mg/ml (288U/ml) collagenase solution was added to give a final collagenase concentration of 5 U/ml (17 μg/ml). The solution was replaced every eight hours to retain enough activity of collagenase. At different time intervals the hydrogels were weighed after the surface water was gently blotted off. Three replicates per sample were tested. The percent residual mass of hydrogels was calculated according to the ratio of initial hydrogel weight to the weight at each time point.

Structural characterization of BPCs by scanning and transmission electron microscopy. Morphology of human donor eye bank corneas obtained from the Eye Bank of Canada was investigated using a scanning electron microscope (SEM, Model S-2250N, Hitachi, Japan). The bioengineered corneas were imaged using a ZEISS SEM (LEO 1550 Gemini). PBS-equilibrated samples were frozen over night at -80 ˚C and then lyophilized for 6 hrs. The samples were cut out

and attached onto metal holders using conductive double-sided tape, and sputter coated with a gold layer for 60 seconds at 0.1 bar vacuum pressure (Cressington Sputter Coater, 108) prior to SEM examination. SEM micrographs were taken at various magnifications at 25kV and 5 kV for human and bioengineered corneas, respectively. For transmission electron microscopy (TEM), BPC materials prior to implantation were removed from chloroform solution, soaked overnight in PBS, and fixed in glutaraldehyde (2 % glutaraldehyde, 0.1 M Na cacodilate, 0.1 M sucrose, pH 7.4) at 4℃ and post fixated with 1% osmium tetraoxide in 0.15 M sodium cacodylate buffer. Resin infiltration and embedding were performed by first dehydrating samples in ascending concentrations of ethanol followed by incubation with propylenoxide for one hour. Gradual infiltration of Epon 812 resin (TAAB, Reading, England) was initiated by incubation of samples in a propylenoxide/Epon (1:1) solution for 2 hours and infiltration in Epon overnight. The samples were placed in Epon and cured in an oven at 60 ℃ for 48 hours to polymerize. Ultrathin (60nm) sections for TEM analysis were cut by a diamond knife, placed on copper grids, and stained with uranyl acetate-lead citrate. TEM sections of the implant material were observed with a transmission electron microscope (Model JEM-1230, JEOL Ltd., Tokyo, Japan).

Evaluation of human corneal epithelial cells growth on bioengineered scaffolds. HCECs (Immortalized human corneal epithelial cells, American Type Culture Collection (ATCC, Manassas, USA) were used to evaluate epithelial coverage. HCECs were seeded on top of 150 mm^2 pieces of BPC material and supplemented with a serum-free medium optimized for the culture of human corneal epithelial cells. (EpiGRO™ Human Ocular Epithelia Complete Media Kit, Millipore, Billerica, MA, USA). Once the control wells became confluent, after approximately 3 days of culture, all wells were stained with the LIVE/DEAD® Viability/Cytotoxicity assay (Invitrogen) according to the standard protocol. The stained cells were photographed with a Zeiss inverted fluorescent microscope using the Zen software (Zeiss). For every field, green and red fluorescence, corresponding to live and dead cells respectively, was documented under a 10x magnification. Microscopic images were taken on days 1, 3, and 5, post-seeding.

Isolation and cultilvation of corneal stroma-derived mesenchymal stem cells (CS-MSCs) and immunophenotyping. All tissue collection complied with the guidelines of the Helsinki Declaration and was approved by the Regional Ethical Committee in Debrecen, Hungary (DEOEC RKEB/IKEB 3094/2010). Central corneal stromas were removed from cadavers within 24 hours from death and debrided of corneal epithelial cells and Bowman's membrane, as well as corneal endothelial cells and Descemet's membrane. Tissue grafts were cut into small (2 x 2 mm) square pieces and plated adherently into 24-well cell culture plates (Costar CLS3527, Sigma) containing Dulbecco-modified Eagle's medium (DMEM, Sigma) supplemented with 10% human AB serum (Sigma) and 200 mM/mL L-glutamine, 10,000 U/mL penicillin- 10 mg/mL steptomycin (Sigma). After the cells reached confluence, 0.025% trypsin-EDTA (1x, Sigma) was used for collection and re-plating of cells into new flasks. At passage 5 (P5), the cells were tested for MSC-antigen expression by fluorescence-activated cell sorting (FACS). A multiparameter analysis of the surface antigen expression of isolated CS-MSCs was performed by three-color flow cytometry using different fluorochrome-conjugated antibodies: CD34, CD45, CD73 (All from BD Biosciences, San Jose, CA, USA), and CD29,

CD90 and CD105 (All from R&D Systems, Minneapolis, MN, USA). After harvesting the cells with 0.025% trypsin-EDTA, cells were washed with normal medium and twice with FACS buffer. The cells were then incubated with antibodies according to manufacturer protocols on ice for 30 min and washed again with FACS buffer and fixed in 1% paraformaldehyde/PBS. The expression of markers was measured by FACSCalibur flow cytometer (BD Biosciences Immunocytometry Systems, Franklin Lakes, NJ) and the data were analyzed using WinMDI software (Joseph Trotter, La Jolla, CA, USA). Results were expressed as means of positive cells (%) ± SEM. Consequently, the CS-MSCs were cultured adherently onto the bioscaffold BPC scaffolds which covered the full bottom of a tissue culture well. Media was changed every alternate day. In addition, the cytoskeletal actin filaments of the CS-MSCs were labeled by phalloidin-TRITC (Sigma-Aldrich), while their nuclei were counterstained by Hoechst (Molecular Probes). The CS-MSCs grown onto and into the BPCs were further stained for Hematoxylin & Eosin (H&E) and imaged using phase-contrast microscopy enhanced by different fluorescent filters for better visualization of the cells and their 3D growth pattern. For cross-sectional localization of CS-MSCs on BPC scaffolds, the BPCs were seeded with CS-MSCs at a 20000 cells/well density and after 21 days, were removed from wells and fixed in 4% paraformaldehyde for 24 hours at 4°C. The cells were then labeled with 1µg/ml propidium iodide, followed by 1 µl/ml FITC-conjugated ConA (Concanavalin A from Canavalia ensiformis) lectin (Vector Labs, Burlingame, CA) labeling for cell surface mannose molecules. For hematoxylin and eosin staining, the samples were sectioned with a rapid freezing method, then placed into silanized slides and observed under a Zeiss Axiovert 70 fluorescence microscope.

Animals and Surgical procedures. 15 male New Zealand white albino rabbits (KB Lidköpings Kaninfarm, Vinninga, Sweden) weighing 3-3.5 kg were used after obtaining approval from the Linköping Animal Research Ethics Committee (Application no. 3-12). All animals were treated following the Association for Research in Vision and Ophthalmology (ARVO) guidelines for the Use of Animals in Ophthalmic and Vision Research. Animals were divided into three groups. In the first (control) group with 5 rabbits, native corneal tissue in one eye was cut intra-stromally with a femtosecond laser but was kept in place and allowed to heal. In the second and third groups (5 rabbits each), the native corneal tissue in one eye was cut in an identical manner, but was thereafter excised and replaced with a BPC. The second group received compression-molded BPCs of 100µm thickness while the third group was implanted with swelled BPCs of 300µm thickness.

Femtosecond laser-assisted intrastromal keratoplasty (FLISK). Surgery was performed under general anesthesia with a 0.5ml/kg mixture of equal poroportions of xylazine (Rompun 20mg/ml; Bayer, Gothenburg, Sweden) and ketamine (Ketalar 50mg/ml; Parke-Davis, Taby, Sweden). Additionally, local anesthetic was given (tetracaine hydrochloride eye drops 1%, Chauvin Pharmaceuticals Ltd., Surrey, UK). An Intralase iFS 150kHz femtosecond laser (Abbott Medical Optics, Solna, Sweden) was used to perform all surgical cuts. Corneal buttons of purely stromal tissue (not including any part of the epithelium or endothelium) were cut by the femtosecond laser. Parameters of laser energy, spot size, lamellar thickness, depth of excision and angle and arc length of the circumferential access cut were chosen based on empirical results of testing with whole porcine eyes. The precise dimensions and location of the buttons to be removed were pre-

programmed via the laser's user interface. For the present study, 3mm diameter buttons of 100µm thick native tissue were to be removed from an approximately mid-stromal depth in the rabbit corneas. Anterior segment optical coherence tomography (Visante OCT, Carl Zeiss AB, Stockholm, Sweden) was used to measure the rabbit corneal thickness in vivo prior to surgery. In the control group, the surgically-cut buttons were left in place in the stroma, whereas buttons were manually excised in groups to receive BPC implants. Excision was achieved by means of an arc-shaped laser cut spanning 70°, following the curvature of the button and extending from the button to the corneal surface (Figure 3). Native tissue was excised manually with surgical forceps, leaving an empty stromal pocket. BPC implants were fabricated in flat, rectangular sheets 10x20mm in size. Sheets in chloroform solution were prepared for surgery by first immersing overnight in PBS, followed by 24h immersion in Minimum Essential Medium solution (Gibco, Life Technologies, Grand Island, NY). Immediately prior to implantation, a 3mm diameter trephine punch was used to cut circular buttons of implant tissue from the flat sheets. The BPC implants were inserted into the prepared stromal pockets by manual insertion of implants sandwiched within surgical forceps (see Results section). Implants were held in place within the host stroma by natural surface tension and intraocular pressure, and no sutures were used. Immediately following surgery and on the first two postoperative days, all operated eyes received antibiotic eye ointment (fucithalmic 1% eye drops, Leo Pharmaceuticals, Denmark).

Postoperative clinical assessment. Immediately following operation, operated eyes were examined in vivo by OCT to assess the femtosecond laser-created pocket and confirm the intra-stromal location of inserted BPC implants. All operated eyes were inspected visually once during the first postoperative week, while under general anesthesia. At 2, 5, and 8 weeks postoperatively, all animals were examined under general anesthesia by OCT, high-magnification digital photography (Nikon D90 camera, Nikon Canada Inc., Toronto, Canada), and by laser-scanning in vivo confocal microscopy (IVCM; Heidelberg Retinal Tomograph 3 with Rostock Corneal Module, Heidelberg Engineering, Heidelberg, Germany). At each examination session, OCT images were taken depicting the same central cross-section of the operated cornea, in high resolution mode. IVCM images were obtained by a technique described in detail elsewhere [17]. Briefly, the instrument's microscope objective (63x/0.95 NA immersion, Zeiss, Oberkochen, Germany) was placed in contact with the topically anesthetized (tetracaine hydrochloride 1%, Chauvin Pharmaceuticals Ltd., UK) rabbit corneal surface by means of a gel coupling medium (Viscotears, carbomer 0.2%, Dr Mann Pharma, Berlin, Germany). The focal depth in the cornea was then adjusted by a joystick-driven motor, to image the epithelium, subbasal nerves, stroma, and endothelium, while manual controls were used to translate the microscope objective to image both the central and peripheral implanted regions. Images were acquired automatically at 8 frames/s and saved directly to hard disk for later retrieval and analysis.

Immunohistochemistry of BPCs *ex vivo*. Following sacrifice, eyes were enucleated and corneas were removed using surgical scissors, fixed in 4% paraformaldehyde fixative solution, and embedded in paraffin. Corneas were prepared with routine methods for paraffin sections (4 µm) and stained with hematoxylin and eosin (H & E). Sections from paraffin-embedded tissues were

deparaffinized with descending concentrations of ethanol and xylene, trypsinized for 5min to retrieve antigen, and endogenous peroxidase was blocked with 3% hydrogen peroxide in methanol. Corneal sections were incubated with the following primary antibodies for 30 minutes at room temperature: mouse monoclonal anti-alpha smooth muscle actin monoclonal antibody, α-SMA (dilution 1:25; ab7817, Abcam, Cambridge, UK); mouse monoclonal anti-type I collagen (1:50; ab6308, Abcam); mouse monoclonal anti-type III collagen (1:100; AF5810, Acris Antibody GmbH, Germany); mouse monoclonal anti-leukocyte common antigen CD45 (1:400; M0701, Dako Sweden AB, Stockholm). The slides were then incubated in envision HRP for 30 minutes following antibody application. 3, 3'-diaminobenzidine (DAB) liquid chromogen was applied for 10 minutes to all samples, and all sections went under counter staining with hematoxylin. Samples were dehydrated through ascending concentrations of ethanol and were finally cleared in xylene and coverslipped with Mountex mounting medium (Histolab Products AB, Gothenburg, Sweden). For double immunofluorescent staining, samples were prepared as above but replacing the endogenous peroxidase blocking step with 5% normal goat serum (Jackson ImmunoResearch Europe, Newmarket, UK). Samples were incubated with the first primary antibody (type III collagen, 1:100) for 30 min. Samples were then rinsed in PBS, blocked, and incubated with the secondary antibody for 30min (goat anti-mouse Dylight 549, 1:100, Jackson ImmunoResearch Europe, Newmarket, UK). This procedure was then repeated with 5% normal donkey serum (Jackson), applying the second primary antibody (α-SMA or CD45) and secondary antibody (donkey anti-mouse Dylight 488, 1:300, Jackson). Imaging was performed using a laser-scanning confocal fluorescence microscope (Nikon Eclipse E600) equipped with 40x/1.30 NA oil-immersion or 20x/0.75 NA objective lenses. Samples were scanned under single or dual laser excitation and a digital camera was used to record images. In all cases, control samples were used and omission of the primary antibody eliminated cell-specific staining.

Transmission electron microscopy (TEM) of BPCs *ex vivo*. For post-implantation ex-vivo analysis, corneal tissue containing implant material was fixed in 4% paraformaldehyde in 0.1M phosphate buffer PBS. The tissue was then washed and further fixed in 2.5% glutaraldehyde containing 0.05% cuprolinic blue (BDH Ltd, Dorset) using a critical electrolyte concentration mode in 25mM sodium acetate with 0.1M magnesium chloride buffer overnight at room temperature. The tissue was then dehydrated through a graded ethanol series (50% to 100%) and 100% acetone. They were then immersed in a mixture of acetone and Spurr's resin for 8 hours. The tissue was further immersed in 100% Spurr's resin for 8 hours (x3) and polymerized in Spurr's resin for 8 hours at 60°C. Ultrathin sections were cut from the polymerized block and these sections were collected on 200 mesh copper grids. Ultrathin sections were stained with 2% uranyl acetate and 2% lead citrate. Sections were observed by transmission electron microscope (Model JEM-1400; JEOL Ltd, Tokyo, Japan).

Statistical analysis. Central corneal thickness as assessed by OCT, was compared over time and between groups using two-way analysis of variance (ANOVA), with time and implant type as independent variables. Post-hoc multiple comparisons were performed with the Student-Newman-Keuls method to isolate specific differences. A two-tailed significance level of less than 0.05 was

considered significant. All statistical tests were performed using Sigma Stat 3.5 statistical software (Systat Software Inc., Chicago, IL, USA).

Results

Mechanical, optical, degradation and structural properties of bioengineered porcine constructs (BPCs). While carbodiimide cross-linking agents such as 1-ethyl-3-(3-dimethylaminopropyl) carbodiimide hydrochloride (EDC) and N-hydroxysuccinimide (NHS) offer low or no toxicity and good cell compatibility, scaffolds made with these agents, due to small size and zero-length cross-links, are often brittle and difficult to surgically manipulate, implant, and suture *in vivo*. Increasing tensile strength and stiffness by an increased dose of cross-linking agent would result in a proportional decrease in elasticity and toughness, due to restriction of the polymer network mobility and an increase in material density [6, 18]. With BPC implants fabricated from high-purity porcine collagen under optimized EDCM/NHS cross-linking ratio and compression molding, we found a 4-fold improvement in mechanical strength and stiffness compared to porcine-based scaffolds we previously reported (Table 1). Moreover, these gains were obtained at the expense of only a modest 0.6-fold decrease in elasticity, and an unexpected 3-fold gain in toughness. Toughness is a critical mechanical property required of materials to withstand surgical implantation. BPC implants were moreover optically transparent at all wavelengths of visible light (Fig. 1*A*). Light transmission for 500 μm thick BPCs was over 90%, comparable to the reported transmission for rabbit and healthy human corneas at the same visible wavelengths [19-21]. Optical light scatter from BPCs was below 6% in the visible range, comparable to scattering from the rabbit cornea at visible wavelengths. To assess the ability of the BPC to degrade over time, an in vitro collagenase assay was used. The degradation rate of the BPC in a 1mg/ml collagenase solution was compared to a non-cross-linked version, and it was found that the BPC was more resistant toward collagenase degradation after cross-linking (Fig. 1*B*). The BPC took 12 hours to degrade by 50%, whereas the non-cross-linked version took about 1 hour. The corresponding time for human corneal tissue in the assay is approximately 4 days [22], indicating that the assay is much more aggressive than the normal *in vivo* corneal environment. Microstructure of a dehydrated human cornea by scanning electron microscopy (SEM) revealed lamellae parallel to the corneal surface, with periodic attachments between layers occurring with 20-100μm periodicity (Fig. 1*C,D*). The BPC microstructure by contrast did not consist of lamellae but of a fine, porous collagen structure sandwiched between two dense surface layers, similar to the anterior 8-12μm thick Bowman's layer and posterior 8-10μm thick Descemet's membrane of the human cornea (Fig. 1*E,F*). Pore size within the BPC ranged from submicron to 2 μm in diameter. Ultrastructural analysis of the BPC by transmission electron microscopy (TEM) revealed a relatively sparse and disorganized, non-lamellar arrangement of collagen fibrils (Fig. 1*G*). Fibrils had varying sizes but were typically 30-40nm in diameter (Fig. 1*H*). Local variations in collagen fibril density were apparent; in some regions, fibrils were not detected, but instead nanometer-sized, electron-dense particulate matter was apparent (Fig. 1*I*). The possibility, however, could not be excluded that variations in collagen fibril size and

density were a sampling phenomenon attributed to the random orientation of the collagen fibrils within the scaffold.

BPCs support colonization and migration of human corneal epithelial cells (HCECs) and human corneal stroma-derived mesenchymal stem cells (CS-MSCs). The BPC was tested for *in vitro* biocompatibility by seeding with immortalized HCECs. The BPC supported attachment and proliferation of HCECs and confluent cell cultures were obtained on day 5 post-seeding (Fig. 2*A*). Human primary CS-MSCs exhibited fibroblastoid, elongated, and spindle-shaped morphology, which formed a monolayer when cultured *in vitro* (Fig. 2*B*) and maintained an active actin cytoskeleton (Fig. 2*C*). By three-color flow cytometry, surface marker phenotype complied with the International Society for Cell Therapy (ISCT) rules defining MSCs: negative for CD34 and CD45, and positive for CD29, as well as positive for CD73 (98.44+2.28%), CD90 (94.78+6.5%) and CD105 (97.67+3.5%) (Fig. 2*D*). When seeded onto the BPC, CS-MSCs formed an adherent monolayer covering the entire BPC surface within 12 days. Attachment and proliferation of CS-MSCs (and/or their derived cells) continued to day 56 (Fig. 2*E*). Moreover, BPC scaffolds remained intact and maintained their 3D structure during the period of cell culture. The ability of the BPC to support a stem cell population as well as the outgrowth of stem cells or their progeny, is important for stem-cell based transplantation to regenerate a damaged area of the cornea. To test for continued cell support and outgrowth, CS-MSC-populated BPCs were re-plated into empty wells. A fraction of CS-MSCs migrated out of some BPCs and into the unpopulated tissue culture plate (Fig. 2*F*). To confirm maintenance of the 3D structure of the BPC after stem cell seeding, BPCs were removed from wells seeded with 20,000 cells/well after 21 days, fixed and stained for hematoxylin and eosin (Fig. 2*G*). The BPC maintained its structure and supported a monolayer of CS-MSCs.

BPCs maintain transparency and thickness in a novel *in vivo* corneal surgical procedure for stromal replacement: femtosecond laser-assisted intra-stromal keratoplasty (FLISK). To test the *in vivo* behavior of cell-free BPCs implanted into the eye with minimal disturbance to epithelium and surrounding host tissue, a new corneal surgical procedure was developed. Surgical extraction of native rabbit corneal tissue was performed using a surgical femtosecond laser (IntraLase iFs 150 kHz, Abbott Medical Optics AB, Stockholm, Sweden). The final surgical model is given schematically in Fig. 3*A*. Using this surgical plan, all surgical cuts, extraction of native host tissue, and insertion of BPCs were completed without complication (see Supplementary Video 1). Post-surgically, BPCs remained in place in all cases without the use of sutures. Duration of surgery was approximately 30 minutes per eye. Immediately following surgery and at 2, 5, and 8 weeks after implantation, cornea cross-sections were examined *in vivo* by anterior segment optical coherence tomography (ASOCT) to assess the ability of the BPC to structurally support the host cornea during healing (Fig. 3*B*). BPCs integrated with the surrounding host tissue and maintained the bulk structure and curvature of the cornea without extensive scarring. At 8 weeks postoperative, the anterior corneal curvature followed that of the posterior cornea in BPC-implanted eyes, similar to autograft controls (where native tissue was cut in situ but not surgically removed). Transparency as assessed by light scattering (bright areas in ASOCT images) was retained in 100µm-thick BPC implants, which had a transparency comparable to autografts (Fig. 3*B*). The swelled 300µm-thick BPC implants had slightly

reduced transparency (elevated scattering) visible on ASOCT scans. To assess the stability of the BPCs in vivo, central corneal thickness was measured by ASOCT (Fig. 3*C*). Central corneal thickness in the native non-operated rabbit cornea was 382 ± 19µm, while autografts did not differ significantly from this value at any time during the postoperative period ($P > 0.05$, one-way ANOVA). Two-way ANOVA revealed no significant difference in thickness between autograft corneas and those with 100µm thick BPCs at any time point, nor any significant change in thickness of autograft or 100µm BPC-implanted corneas over time ($P > 0.05$ for both). The analysis also revealed that implantation of the initially 300µm-thick swelled BPCs resulted in significantly thicker corneas at all postoperative time points relative to the other groups ($P < 0.001$). Corneas with 300µm-thick swelled BPCs underwent significant thinning from 2 to 5 weeks ($P < 0.001$), but stabilized at 5 weeks with no further reduction in thickness ($P = 0.68$) and had a final central thickness of 478 ± 42µm, approximately 100 µm thicker than the native rabbit cornea. Under clinical examination, corneas with autografts and 100µm thick BPCs were transparent at 2 weeks, and maintained this transparency to 8 weeks, with the circular border of the BPC barely visible (Fig. 3*D*). The 300µm swelled BPCs, however, exhibited some residual translucency (corneal haze) at 2 weeks, that remained at 8 weeks (Fig. 3*D*). Results for the swelled BPCs were not unexpected as 300µm-thick BPCs had the same total amount of collagen as the 100µm-thick BPCs, but were allowed to swell during curing, resulting in a more porous structure enabling a greater degree of hydration, mimicking an edematous cornea *in vivo*.

FLISK maintains the host cellular environment while BPCs integrate and attract host cells *in vivo*. Corneal examination at the cellular level by in vivo confocal microscopy revealed that during the postoperative period, the anatomic structures of the cornea outside the implanted zone were left undisturbed by the surgery or by the presence of the BPC (Fig. 4). All anatomic layers including epithelium, subbasal epithelial (sensory) nerves, stromal keratocytes and endothelium were detected and exhibited normal morphology at 8 weeks postoperative. Moreover, no inflammatory cells could be observed *in vivo*. Within the surgical zone, laser cut interfaces (autograft) or implant-host interfaces (anterior, posterior and lateral) were marked by light-scattering cells (activated keratocytes and fibroblasts) and light-scattering tissue (fibrous scar tissue). Within the center of the surgical zone in autografts, slight activation and deformation of stromal keratocytes were evident. The center of the BPC implants remained unpopulated by cells at 8 weeks. Some cells, however, were observed within the BPCs in peripheral areas near the host-to-biomaterial implant border (Fig. 4).

BPCs enable rapid wound healing without inflammation, and initiate stromal regeneration by host myofibroblast recruitment. In autografts, where tissue was laser cut (but not extracted), remnants of the lamellar laser incisions were visible (Fig. 5*A,D,G,J*). In autografted corneas, minimal presence of α-SMA$^+$ stromal myofibroblasts or type III collagen (scar-type collagen) was found at the lamellar interfaces , and no CD45$^+$ leukocytes were observed around the surgrical zone. In corneas with BPCs, the BPC was discernible by its homogeneous and acellular appearance (Fig. 5*B,C*). BPCs remained intact and integrated with surrounding host tissue, with α-SMA$^+$ stromal myofibroblasts often observed in close apposition to anterior and posterior lamellar interfaces (Fig.

5*E,F*). These myofibroblasts appeared in regions where type III collagen was present. No $CD45^+$ leukocytes were observed in or around the BPCs. To determine whether the myofibroblasts were the source of the type III collagen and to confirm the absence of inflammatory leukocytes, co-localization of α-SMA/type III collagen and type III collagen/CD45 was investigated by double immunofluorescent staining (Fig. 5*M-R*). At anterior and posterior lamellar interfaces, $\alpha\text{-SMA}^+$ myofibroblasts, in close proximity to and often in direct contact with the BPC, co-localized with new type III collagen. No strong $CD45^+$ signal was observed, indicating no association of new collagen production with leukocyte invasion. Closer inspection of the BPC periphery in H&E and immunostained sections indicated migration of a limited number of stromal cells into the implant at 8 weeks postoperative (Fig. 5*S-Z*). Cells appeared to migrate into BPCs in single file through narrow tunnels (Fig. 5*S,T*), single cells appeared deeper within the BPC (Fig. 5*U*), or cells appeared to invade the BPC from peripheral locations (Fig. 5*V-Z*). These cells were associated with the production of type III collagen within the implants, and a limited transformation of BPC collagen into host collagen was visible in H&E stained sections (Fig. 5*Y,Z*).

BPCs contain proteoglycans but no detectable collagen fibril structure or lamellae despite maintaining transparency *in vivo*. At 8 weeks postoperative, *ex vivo* transmission electron microscopy of implanted corneas revealed the lamellar laser-cut interface as a dark, electron-dense demarcation line (Fig. 6*A,B*). On the host side of this line, the new type III collagen appeared as a band of tissue with disrupted fibril structure interspersed with dark vacuoles (Fig. 6*D,E*). Stromal cells (myofibroblasts) with well-developed nuclei and endoplasmic reticulum were observed in association with the modified collagen band, and close to the implant-to-host interface (Fig. 6*B*). Outside this band, tightly-packed and perpendicularly-oriented collagen fibrils within lamellae were visible and were characteristic of the normal, native corneal stroma (Fig. 6*C,E*). The BPC, however, consisted of a homogeneous, non-lamellar ultrastructure (Fig. 6*A,B,F*). Even at high magnification, no collagen fibril structure was observed within the BPC, while electron lucent spaces were present (Fig. 6*F*). Proteoglycans (analyzed in TEM sections not stained with uranyl acetate and lead citrate) in the host stroma were regularly arranged around parallel-running collagen fibrils (Fig. 6*G*). Unexpectedly, the BPC also contained proteoglycans; however, these were randomly distributed (Fig. 6*H*).

Discussion

The requirements of bioengineered materials for vision-restoring therapeutic application in the cornea are stringent: materials must be strong and implantable, transparent, immune-compatible, and robust enough to maintain shape and transparency *in vivo*. However, in order to stimulate the host cornea to regenerate, a scaffold material must support cell invasion and turnover into host extracellular matrix. Additionally, scaffolds should be low-cost and sourced from widely available, high-purity raw materials. While earlier human collagen-based scaffolds have had some success in preclinical models [7] and in a clinical phase I study [8], widespread adoption will require a shift from specialized and expensive niche materials to high-availability, low-cost, medical-grade raw materials. Porcine skin collagen is both biologically and commercially abundant, and can be

obtained with high purity and at low cost. EDC-NHS crosslinked collagen materials have previously been made with lower collagen content [6] and suboptimal mechanical strength, resulting in premature thinning [8] instead of rapid recruitment of stromal cells. Previous collagen-based materials have been anchored to surrounding host tissue by fibroblast attachment at the periphery [8,23], while a true stromal regeneration by host cells producing new collagen from within the scaffold was not apparent histochemically, even 4 years post-implantation [23,24]. Previous materials may not have had the strength or enzymatic resistance to enable cell invasion without complete degradation. Here, the BPCs exhibited a significant improvement in mechanical properties relative to earlier versions without increasing the concentration of cross-linkers; the relative proportion of cross-linkers to collagen was actually reduced over 4-fold compared to earlier materials [6]. Improved mechanical properties were likely due to optimization of the scaffold formulation and fabrication process to support high collagen content, the use of higher molecular weight EDCM (MW 297) as opposed to the traditional EDC (MW 191), and high purity of the raw porcine collagen. To our knowledge, this is the first report of a high, 18% collagen solution that is fully transparent and used for the fabrication of tissue-engineered corneal implants, and it is additionally the first time we are reporting the use of EDCM instead of EDC. The higher molecular weight of the crosslinker appeared to slow down the covalent bonding kinetics which may allow better mobility in the surrounding hydrogel to result in EDCM molecules traveling further into the intra-fibrillar spaces to reach more crosslinking sites on collagen. The result is avoidance of premature gelling and a more brittle hydrogel that would occur with faster crosslinking. The use of EDCM instead of EDC, combined with the high-purity collagen (increased number of crosslinking sites) likely had a significant impact on mechanical properties of the hydrogels, resulting in more robust corneal scaffolds.

Despite the significantly higher strength, toughness, elasticity, and resistance to collagenase degradation exhibited by the human cornea compared to BPCs, our *in vivo* data suggest it may not be desirable for bioengineered materials to closely mimic the mechanical characteristics of the native cornea. While human donor corneal tissue may take years to become cell-repopulated after transplantation [25], here we observed an early cell migration into BPCs and initial collagen transformation only 8 weeks after implantation. Although the migration was limited, with longer follow-up, increased cell invasion is to be expected. Contrary to a widely accepted belief in tissue engineering, this illustrates that tissue-mimetic scaffolds do not necessarily need to closely match the mechanical properties of their natural counterparts.

Corneal stromal regeneration *in vivo* by host stromal cell recruitment was observed, a phenomenon that has been difficult to clearly demonstrate in earlier studies. In earlier studies, stromal cell invasion of implanted biomaterials has been shown, but the production of new collagen by these invading cells has not been convincingly demonstrated [8, 23, 24, 26-28]. The BPC also supported human corneal epithelial cell growth and a human corneal stroma-derived mesenchymal stem cell population *in vitro*. When combined with an optimal seeding method and temporal degradation profile, cell-seeded BPCs could find additional therapeutic applications in stem cell-mediated corneal tissue regeneration for blinding conditions associated with epithelial stem cell deficiency

[29] or disorders of the corneal stroma [30,31]. A major problem for stem cell delivery in the cornea has been the lack of a suitable carrier for the stem cells – one that can maintain a population of stem cells while simultaneously enabling migration of the cells or their progeny into surrounding host tissue. In this respect, the BPC could be a promising vehicle for stem cell delivery; however, further in vitro studies are required to characterize the stem cell characteristics after interaction with the BPC.

In addition to the modulation of mechanical and biological properties, the BPC material system allows physical properties such as implant size, thickness, swelling, and degradability to be tuned for a particular application. In this study, 300µm thick swelled BPCs were suboptimal in terms of *in vivo* optical transparency and maintenance of total corneal thickness, leading us to favor the use of a compression molding technique. Swelled implants, however, demonstrate the ability to use thicker BPCs to substantially thicken the corneal stroma, for treatment of conditions such as corneal ectasia, ulceration, and keratoconus. Additionally, the use of overly thick implants provides useful data on the duration and amount of *in vivo* thinning mediated by factors such as enzymatic degradation, intraocular pressure, and de-hydration of implants due to, for example, the mechanical effect of eyelid motion. The majority of thinning of the thick BPCs occurred during the first five postoperative weeks, after which corneal thickness stabilized.

By contrast, the compression-molded BPCs with thickness matching that of the excised native tissue exhibited optimal stability and transparency *in vivo*, mimicking native autografts. During the entire postoperative healing phase, BPCs maintained transparency and did not provoke an immune response despite the absence of postoperative immunosuppressive medication. This immune-compatibility was likely due to the non-immunogenic nature of the purified porcine collagen, and the implantation of cell-free BPCs, as it has been shown in a large series of human corneal transplantations that cryopreservation of donor tissue (which kills all donor cells) virtually eliminates immune rejection postoperatively [32].

An unexpected result in this study was the absence of an ordered arrangement of intact collagen fibrils in the 100µm thick BPCs, despite their transparency. The healthy human cornea is comprised of about 200 layers of distinct collagenous lamellae densely packed together, each lamella 1-2 µm thick and comprised of collagen fibrils about 36 nm in diameter [21, 33]. The prevailing theory for the physical origin of corneal transparency is that collagen fibrils are spaced regularly in three dimensions and that the distance between the collagen fibrils is similar to the diameter of a fibril itself [34,35]. By these criteria, the BPC microstructure should render the material opaque; however, the BPC had a transmission superior to the human donor cornea *in vitro*, and similar transparency to autografts (native rabbit tissue) *in vivo*, despite a porous, non-lamellar architecture and absence of collagen fibril ultrastructure. Moreover, proteoglycans were distributed throughout the BPC, which are thought to play a role in maintaining corneal transparency by regulating the assembly of collagen fibrils and organization of the extracellular matrix [36]. The origin of the transparency of the BPC and the composition of the proteoglycans bound within its matrix warrants closer investigation.

Another notable finding in this study was the successful implementation of FLISK to excise and replace stromal tissue. Compared to earlier studies with poorer retention with techniques requiring extensive suturing [26,27], the FLISK technique resulted in a 100% implant retention rate in 15 rabbit corneas. The procedure maintained epithelial integrity and resulted in rapid wound healing without inflammation and without the use of surgical sutures, thereby avoiding the potentially damaging effects of the epithelial wound healing response [37]. In recent years, corneal transplantation has evolved from replacing the entire thickness of the cornea (penetrating keratoplasty) for all indications, to replacing only the damaged or diseased corneal layers, either the endothelium (endothelial keratoplasty) or the epithelium and stroma (deep anterior lamellar keratoplasty) [38-40]. These new partial replacement techniques have been rapidly adopted by surgeons worldwide, due to their potential for excellent postoperative healing and improved visual outcomes [41, 42]. In this study, FLISK presents a new surgical option, intra-stromal keratoplasty, that is not only applicable for testing stromal regeneration in implanted biomaterials, but could have wider applicability in corneal surgery. Although only one-third of the corneal stromal thickness was replaced in this study, the femtosecond laser could be programmed to excise a greater proportion of the stroma to treat conditions such as stromal scarring, corneal dystrophies, or keratoconus. Advantages of the procedure are the avoidance of sutures, maintenance of the epithelial barrier and thereby a rapid wound healing response, minimal disruption of endothelium, and reducing the possibility for postoperative rejection [43].

Further testing BPCs can be extended to thicker implants and surgical procedures such as lamellar keratoplasty, in order to validate BPC implants in a model closer to the final clinical application. The robust material and biological properties of BPCs, however, combined with the availability and high quality of raw materials, is compatible with producing BPCs in quantities required for addressing the high demand for suitable donor tissue.

Acknowledgements

The authors wish to sincerely thank Dr. Amy Gelmi for SEM imaging, Dr. Adrian Elizondo for HCEC work, Mohammad Mirazul Islam for assistance with the collagenase assay, Gertrud Strid for assistance with tissue sample preparation, and Catharina Traneus-Röckert for immunostaining of cornea sections. The authors wish to additionally acknowledge the kind contribution of Abbott Medical Optics (Sweden and UK affiliates) for technical assistance in the development of the FLISK procedure, which is presently an off-label use of the IntraLase iFs 150 kHz femtosecond laser. The authors would also like to extend their sincere appreciation to the Deanship of Scientific Research at King Saud University for its funding of this research through the Research Project no 'RGP – VPP – 219'. This study was also made possible with funding from the Swedish Research Council, the County Council of Östergötland, Sweden, the Freemason's Foundation, and Crown Princess Margareta's Foundation for the Visually Impaired. The authors would also like to acknowledge the EU FP7 COST action BM-1302.

Author Disclosure Statement

One author of this publication (Mehrdad Rafat) holds stock in the company LinkoCare Life Sciences AB, which is a start-up/spin-off of Linköping University and is developing products related to the research being reported, and holds relevant patents. Mehrdad also serves on the Board of Directors of the company. The terms of his arrangements have been reviewed and approved by Linköping University in accordance with its policy on objectivity in research.
For the remaining authors, no competing financial interests exist.

Author Contributions

Designed research: MK, MR, GP, PF, NL. Performed research: MK, MR, ZV, PF, NL. Contributed analytic tools: MK, MR, GP, ZV, SA, NL. Analyzed data: MK, MR, GP, SA, PF, NL. Wrote the paper: MR, GP, NL.

References

1. World Health Organization Global Data on Visual Impairments 2010, url: http://www.who.int/blindness/GLOBALDATAFINALforweb.pdf , accessed Sept 30, 2013.

2. Whitcher, J.P., Srinivasan, M., and Upadhyay, M.P. Corneal blindness: a global perspective. Bull World Health Organ **79**, 214, 2001.

3. World Health Organization, url: http://www.who.int/blindness/causes/priority/en/index9.html, accessed Aug 28, 2013.

4. Li, F., Carlsson, D., Lohmann, C., Suuronen, E., Vascotto, S., Kobuch, K., et al. Cellular and nerve regeneration within a biosynthetic extracellular matrix for corneal transplantation. Proc Natl Acad Sci USA **100**, 15346, 2003.

5. Liu, Y., Gan, L., Carlsson, D.J., Fagerholm, P., Lagali, N., Watsky, M.A., et al. A simple, cross-linked collagen tissue substitute for corneal implantation. Invest Ophthalmol Vis Sci **47**, 1869, 2006.

6. Rafat, M., Li, F., Fagerholm, P., Lagali, N.S., Watsky, M.A., Munger, R., et al. PEG-stabilized carbodiimide cross linked collagen-chitosan hydrogels for corneal tissue engineering. Biomaterials **29**, 3960, 2008.

7. Merrett, K., Fagerholm, P., McLaughlin, C.R., Dravida, S., Lagali, N., Shinozaki, N., et al. Tissue engineered recombinant human collagen-based corneal substitutes for implantation: performance of type I vs type III collagen. Invest Ophthalmol Vis Sci **49**, 3887, 2008.

8. Fagerholm, P., Lagali, N.S., Merrett, K., Jackson, W.B., Munger, R., Liu, Y., et al. A biosynthetic alternative to human donor tissue for inducing corneal regeneration: 24 month follow-up of a Phase I clinical study. Sci Transl Med **2**, 46ra61, 2010.

9. Griffith, M., Jackson, W.B., Lagali, N., Merrett, K., Li, F., and Fagerholm, P. Artificial corneas: a regenerative medicine approach. Eye **23**, 1985, 2009.

10. Pang, K., Du, L., and Wu, X. A rabbit anterior cornea replacement derived from acellular porcine cornea matrix, epithelial cells and keratocytes. Biomaterials **31**, 7257, 2010.

11. Du, L., and Wu, X. Development and characterization of a full-thickness acellular porcine cornea matrix for tissue engineering. Artif Organs **35**, 691, 2011.

12. Zhou, Y., Wu, Z., Ge, J., Wan, P., Li, N., Xiang, P., et al. Development and characterization of acellular porcine corneal matrix using sodium dodecylsulfate. Cornea **30**, 73, 2011.

13. Yoeruek, E., Bayyoud, T., Maurus, C., Hofmann, J., Spitzer, M.S., Bartz-Schmidt, K.U., et al. Decellularization of porcine corneas and repopulation with human corneal cells for tissue-engineered xenografts. Acta Ophthalmol **90**, e125, 2012.

14. RMS Innovations U.K. Limited Corp. Url: http://www.rmsbio.net/collagen/theraform.asp accessed 30 Sept, 2013.

15. Life Spring BioTech Co., Ltd.(Taiwan). Url: http://www.lsbiotek.com/eng/index.php accessed 27 Feb, 2014.

16. Priest, D., and Munger, R. A new instrument for the monitoring of the optical properties of corneas. Invest Ophthalmol Vis Sci **39**(suppl), s352, 1998.

17. Lagali, N., Griffith, M., and Fagerholm, P. In vivo confocal microscopy of the cornea to assess tissue regenerative response after biomaterial implantation in humans. Methods Mol Biol **1014**, 211, 2013.

18. Olde Damink, L.H., Dijkstra, P.J., van Luyn, M.J., van Wachem, P.B., Nieuwenhuis, P., and Feijen, J. Cross-linking of dermal sheep collagen using a water-soluble carbodiimide. Biomaterials **17**, 765, 1996.

19. Meek, K.M., Leonard, D.W., Connon, C.J., Dennis, S., and Khan, S. Transparency, swelling and scarring in the corneal stroma. Eye **17**, 927, 2003.

20. Beems, E.M., and van Best, J.A. Light transmission of the cornea in whole human eyes. Exp Eye Res **50**, 393, 1990.

21. Freegard, T.J. The physical basis of transparency of the normal cornea. Eye **11**, 465, 1997.

22. Liu, W., Deng, C., McLaughlin, C.R., Fagerholm, P., Lagali, N.S., Heyne, B., et al. Collagen-phosphorylcholine interpenetrating network hydrogels as corneal substitutes. Biomaterials **30**, 1551, 2009.

23. Fagerholm P, Lagali NS, Ong JA, Merrett K, Jackson WB, Polarek JW, Suuronen EJ, Liu Y, Brunette I, Griffith M. Stable Corneal Regeneration Four Years After Implantation of a Cell-Free Recombinant Human Collagen Scaffold. Biomaterials **35**, 2420, 2014.

24. Lagali N, Fagerholm P, Griffith M. Biosynthetic corneas – prospects for supplementing the human donor cornea supply. Expert Rev Med Devices **8**, 127, 2011.

25. Lagali, N., Stenevi, U., Claesson, M., Fagerholm, P., Hanson, C., Weijdegård, B., et al. Survival of donor-derived cells in human corneal transplants. Invest Ophthalmol Vis Sci **50**, 2673, 2009.

26. Xu Y, Xu Y, Huang C, Feng Y, Li Y, Wang W. Development of a rabbit corneal equivalent using an acellular corneal matrix of a porcine substrate. Mol Vis **14**, 2180, 2008.

27. Builles N, Janin-Manificat H, Malbouyres M, Justin V, et al. Use of magnetically oriented orthogonal collagen scaffolds for hemi-corneal reconstruction and regeneration. Biomaterials **31**, 8313, 2010.

28. Duncan TJ, Tanaka Y, Shi D, Kubota A, Quantock AJ, Nishida K. Flow-manipulated, crosslinked collagen gels for use as corneal equivalents. Biomaterials **31**, 8996, 2010.

29. Tsai, R.J.F., Li, L.M., and Chen, J.K. Reconstruction of Damaged Corneas by Transplantation of Autologous Limbal Epithelial Cells. N Engl J Med **343**, 86, 2000.

30. Marcon, A.S., Cohen, E.J., Rapuano, C.J., and Laibson, P.R. Recurrence of corneal stromal dystrophies after penetrating keratoplasty. Cornea **22**, 19, 2003.

31. Chen, H., Pires, R., and Tseng, S. Amniotic membrane transplantation for severe neurotrophic corneal ulcers. Br J Ophthalmol **84**, 826, 2000.

32. Cottle, F., Benson, W., and Goosey, J. Incidence of graft rejection following lamellar keratoplasty. Invest Ophthalmol Vis Sci **39**, S1069, 1998.

33. Craig, A.S., Robertson, J.G., and Parry, D.A. Preservation of corneal collagen fibril structure using low-temperature procedures for electron microscopy. J Ultrastruct Mol Struct Res **96**, 172, 1986.

34. Silver, F.H., and Christiansen, D.L. Biomaterials science and biocompatibility. New York: Springer, 1999.

35. Hassell, J.R., and Birk, D.E. The molecular basis of corneal transparency. Exp Eye Res **91**, 326, 2010.

36. Michelacci, Y.M. Collagens and proteoglycans of the corneal extracellular matrix. Braz J Med Biol Res **36**, 1037, 2003.

37. Wilson, S.E., Mohan, R.R., Mohan, R.R., Ambrósio, R. Jr., Hong, J., and Lee, J. The corneal wound healing response: cytokine-mediated interaction of the epithelium, stroma, and inflammatory cells. Prog Retin Eye Res **20**, 625, 2001.

38. Melles, G.R., Lander, F., Rietveld, F.J., Remeijer, L., Beekhuis, W.H., and Binder, P.S. A new surgical technique for deep stromal, anterior lamellar keratoplasty. Br J Ophthalmol **83**, 327, 1999.

39. Anwar, M., and Teichmann, K.D. Big-bubble technique to bare Descemet's membrane in anterior lamellar keratoplasty. J Cataract Refract Surg **28**, 398, 2002.

40. Price, F.W. Jr., and Price, M.O. Descemet's stripping with endothelial keratoplasty in 50 eyes: a refractive neutral corneal transplant. J Refract Surg **21**, 339, 2005.

41. Kosker, M., Suri, K., Duman, F., Hammersmith, K.M., Nagra, P.K., and Rapuano, C.J. Long-term outcomes of penetrating keratoplasty and Descemet stripping endothelial keratoplasty for Fuchs endothelial dystrophy: fellow eye comparison. Cornea **32**, 1083, 2013.

42. Price, M.O., and Price, F.W. Jr. Descemet's membrane endothelial keratoplasty surgery: update on the evidence and hurdles to acceptance. Curr Opin Ophthalmol **24**, 329, 2013.

43. Sharma, N., Kandar, A.K., and Singh Titiyal, J. Stromal rejection after big bubble deep anterior lamellar keratoplasty: case series and review of literature. Eye Contact Lens **39**, 194, 2013.

Name and contact information for reprints:

Neil Lagali, PhD
Department of Ophthalmology
Institute for Clinical and Experimental Medicine
Linköping University
581 83 Linköping, Sweden
Tel +46 101034658
Fax +46 101033065
Email: neil.lagali@liu.se

Table

Table 1 Mechanical properties of the bioengineered porcine construct (BPC) compared to an earlier reported porcine collagen-based material with lower collagen content, and a human donor cornea.

Construct	Ultimate Stress [Strength] (kPa)	Ultimate Elongation [Elasticity] (%)	Elastic Modulus [Stiffness] (MPa)	Energy to Break [Toughness] (kPa)
BPC (18% collagen)	**446.4 ± 3.0**	**23.5 ± 0.11**	**3.29 ± 0.34**	**40.3 ± 0.1**
Porcine scaffold (10% collagen)[a]	112.0 ± 16.0	38.0 ± 2.5	0.72 ± 0.09	13.7 ± 2.5
Human Donor Cornea[a]	3294.0 ± 194.0	60.0 ± 15.0	15.86± 1.96	980.0 ± 200.0

[a] data from reference [6].

Figures

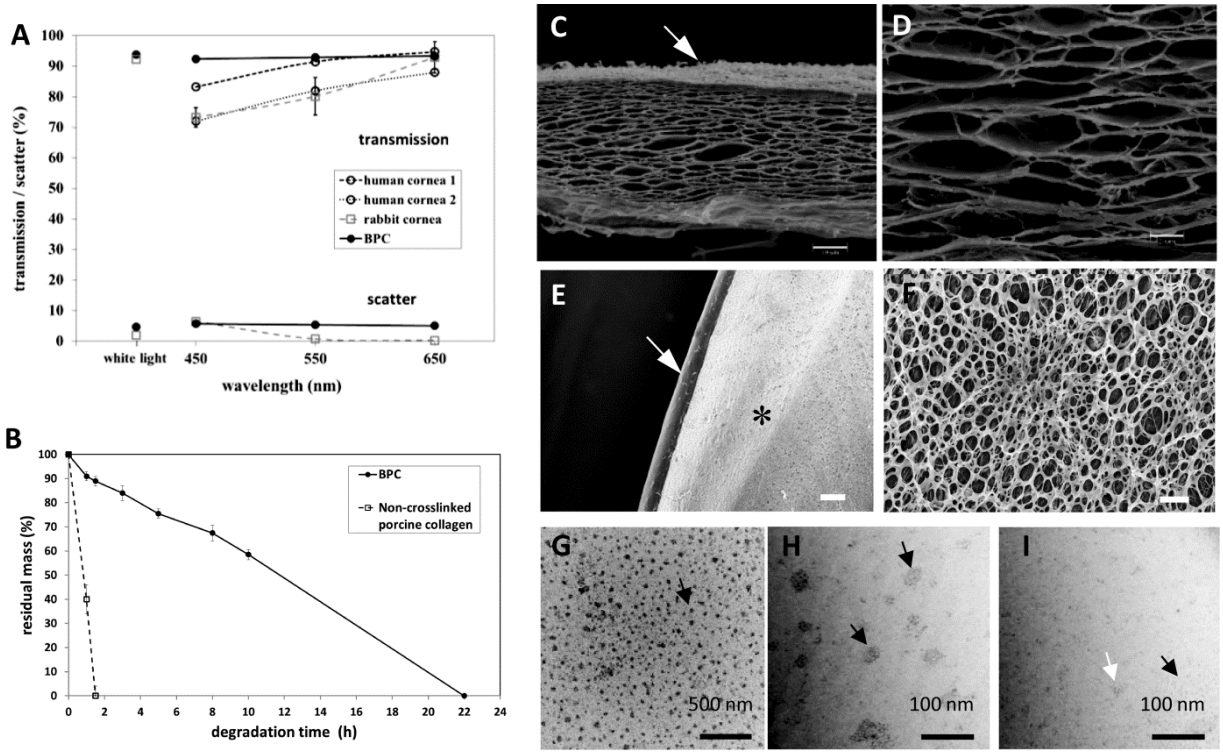

Fig. 1. Optical, chemical, and structural characterization of the bioengineered porcine construct (BPC). (A) Optical transmission and scatter through a 500 µm-thick BPC at visible light wavelengths vs. rabbit and human corneas. Data for human and rabbit corneas was taken from refs [19-21]. Error bars represent standard deviation (SD) of 3 samples per wavelength. (B) Degradation rate of the BPC implant and a non-cross-linked porcine collagen film in collagenase solution. Error bars indicate SD of 3 samples per time point. (C) Scanning electron microscope (SEM) image of a dehydrated human cornea in cross section, indicating denser surface layers (arrow). (D) High magnification view of (C), depicting intra-lamellar attachments. (E) SEM image of a BPC indicating a surface collagen layer (arrow) denser than the bulk material (asterisk). (F) High magnification view of the bulk BPC structure, depicting a fine, porous collagen mesh structure without visible lamellae. (G-I) Transmission electron microscopy of the BPC. (G) Random distribution of collagen fibrils viewed in cross-section (arrow). (H) At higher magnification, collagen fibrils were observed to be 30-40nm in diameter (arrows), while in some regions (I) fibrils were absent and electron-dense inclusions (white arrow) or nanometer-sized electron-dense particulate matter (black arrow) was observed. Scale bars: (C) 100µm; (D) 20µm; (E) 20µm; (F) 2µm.

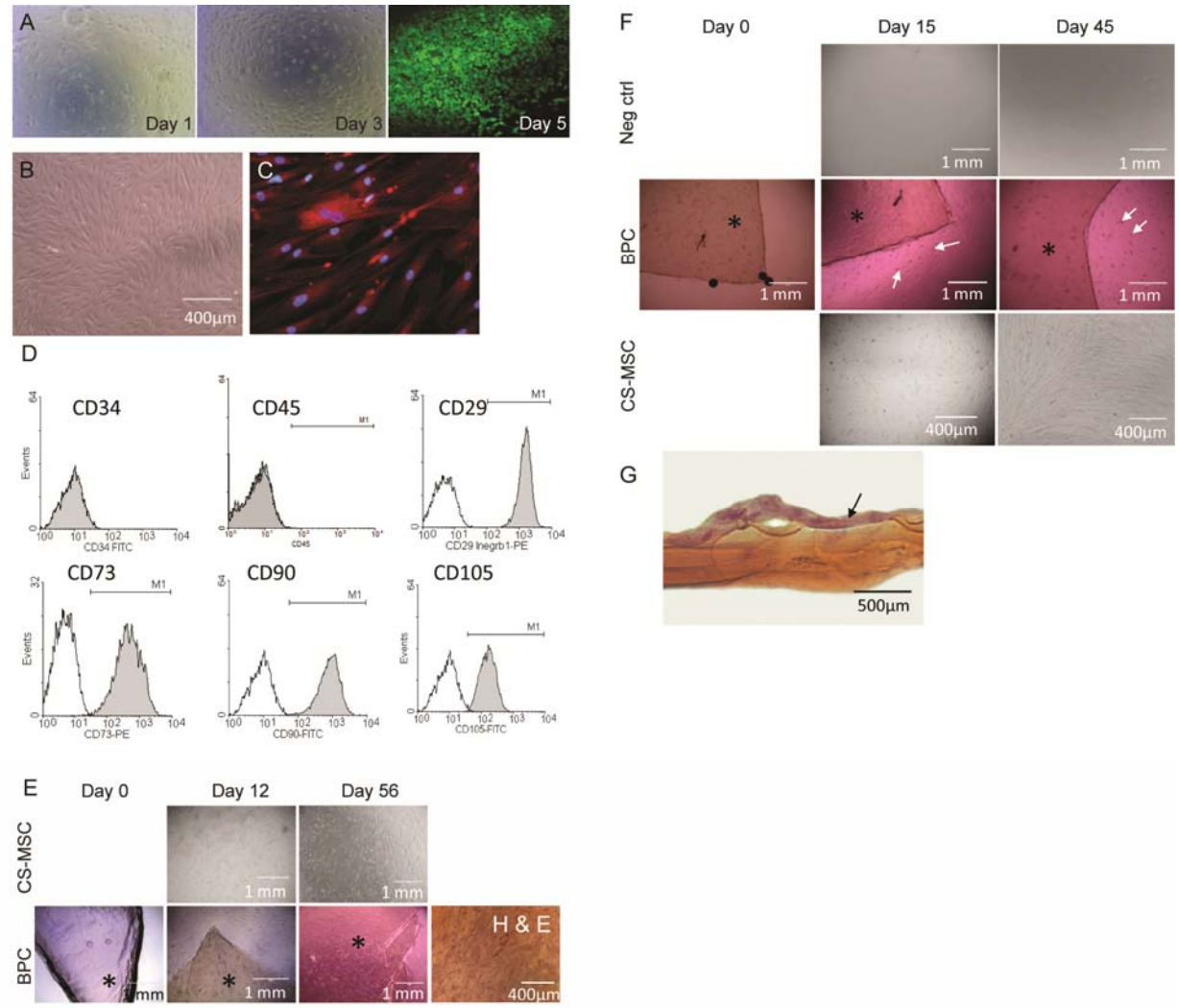

Fig. 2. BPCs support colonization and migration of human corneal epithelial cells (HCECs) and human corneal stroma-derived mesenchymal stem cells (CS-MSCs). (A) HCECs attached to the BPC implants as indicated by light microscopy on day 1 and day 3 post-seeding, and reached confluence on day 5 as indicated by fluorescent microscopy using the LIVE/DEAD® assay. (B) The CS-MSCs showed fibroblastoid morphology and actin cytoskeletal structure (C) in monolayer cell cultures. (D) CS-MSC phenotype was confirmed by three-color flow cytometry. (E) When seeded at 20000 cells/well on BPC (asterisk), CS-MSCs migrated onto the BPC (asterisk) within 12 days. Original magnification: 40x and 200x. (F) CS-MSCs grown onto BPCs were re-plated for adherent growth into empty wells to examine their repopulation potential. A proportion of cells migrated out of some BPCs at days 15 and 45 (white arrows), but did not fully repopulate the free area when compared to non-scaffold grown CS-MSCs. (G) When CS-MSCs were seeded onto BPCs at 20000 cells/well, they formed a thin monolayer on the BPC surface after 21 days (black arrow). A flash-frozen section stained by hematoxylin and eosin is shown. (H) The CS-MSCs on the BPC carrier was further visualized by ConA lectin- and propidium iodide staining under a fluorescent microscope. Whole thickness BPCs with CS-MSCs were z-stacked and reconstructed and shown in ZX, YX and ZY

directional views. Localization of fluorescence to the sample surface (white arrows) confirmed a monolayer of cells (original magnification x20).

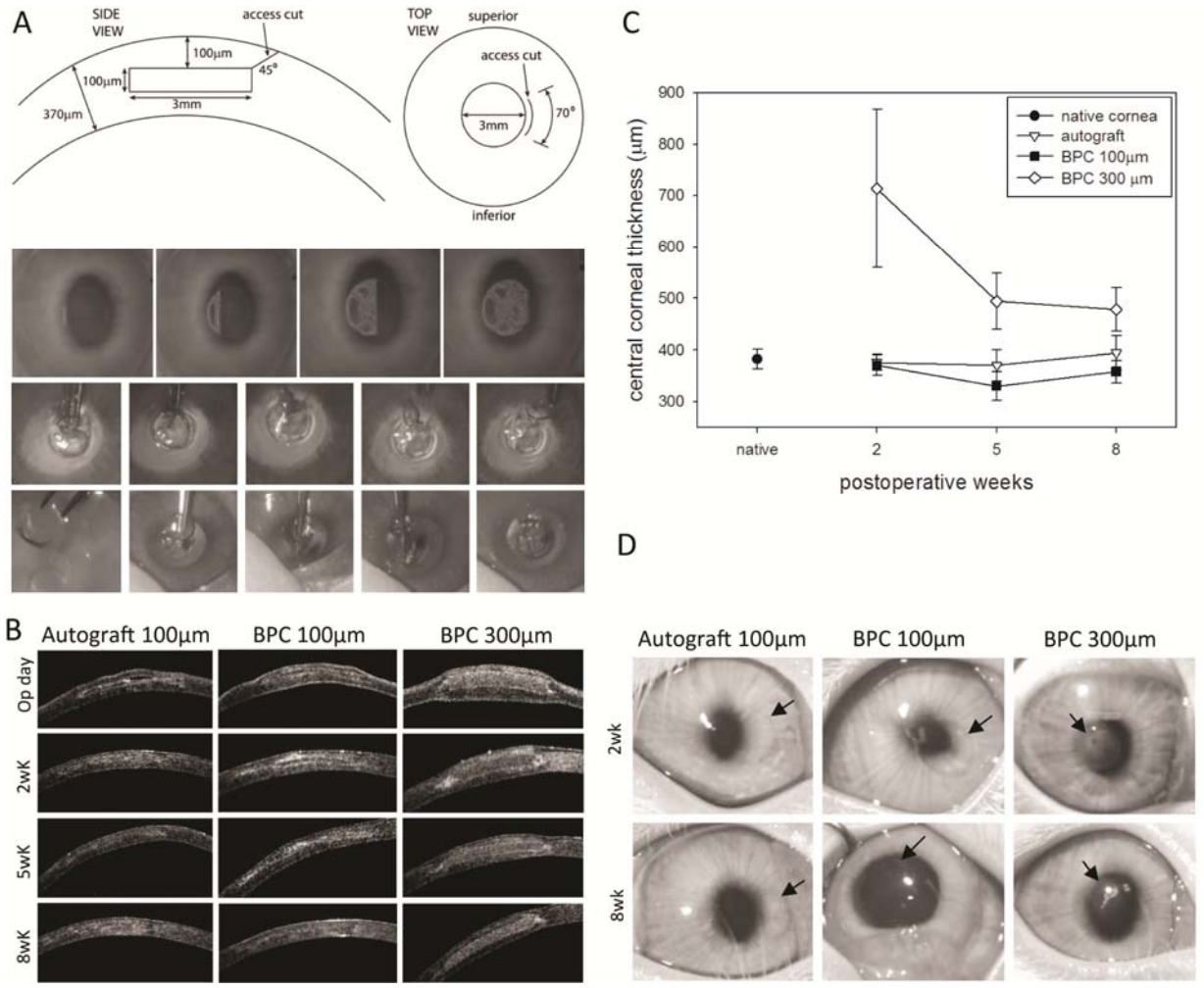

Fig. 3. Procedure of femtosecond laser-assisted intra-stromal keratoplasty (FLISK) and BPC structural and optical characterization *in vivo*. (A) schematic of the surgical plan. A disc of native tissue 100µm thick and 3mm in diameter is removed from the mid-stroma via a small access cut to the corneal surface. The access cut spans a 70° arc and is oriented 45° to the plane of the disc. First row: time series of the first posterior lamellar cut made by the femtosecond laser spot that is swept across the cornea in a raster fashion. The circular side cut, anterior lamellar cut, and access cut are not shown. Second row: extraction of the native stromal disc of tissue using surgical forceps. Third row: insertion of the BPC into the mid-stromal pocket using surgical forceps (see Supplementary Video 1). (B) Longitudinal ASOCT images of the same implanted corneas over the 8-week postoperative period. Surface irregularities immediately after operation had normalized by 2 weeks, and complete corneal curvature was restored by 8 weeks. The 100µm-thick BPCs mimicked autograft transparency and curvature, while the 300µm-thick swelled BPCs had slightly reduced transparency. (C) In vivo central corneal thickness measured by ASOCT. Results shown are the mean and standard deviation (error bars) of measurements from 5 corneas per group at each time point. (D) Clinical *in vivo* photographs of the same corneas at 2 and 8 weeks postoperative. Corneas were transparent in the autograft and 100µm thick BPC groups, with the circular boundary of the

implants barely visible (arrows, first two columns). In the 300µm thick BPC group, some corneal haze was visible at 2 weeks, that persisted to 8 weeks (arrows, third column).

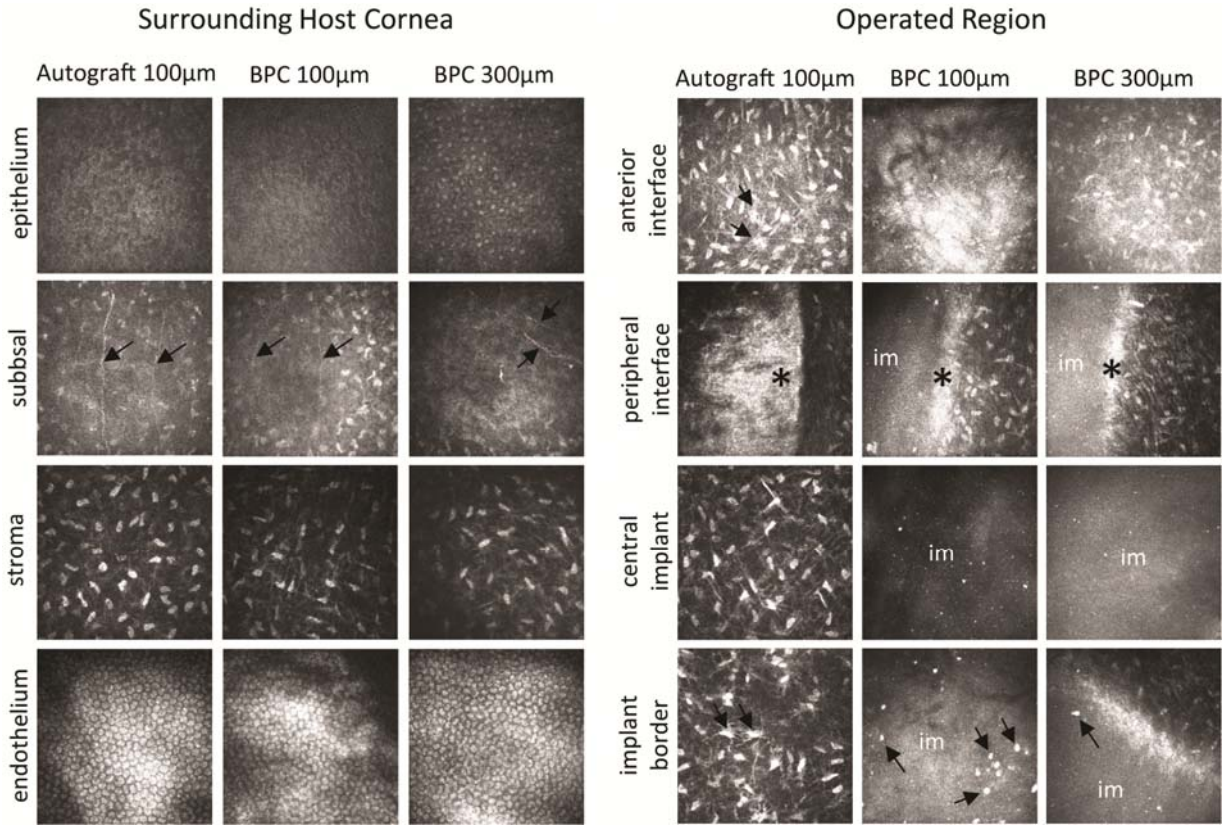

Fig. 4. In vivo confocal microscopy of the cornea in live rabbit corneas 8 weeks postoperative, outside and within the implanted zone. Upper panels: *in vivo* appearance of the central cornea anterior and posterior to the implanted zone. In autografts and in both BPC implanted groups, the central corneal epithelium, subbasal nerves (arrows), stromal keratocytes and endothelium were left undisturbed by the surgical procedure or by the presence of BPCs. All images 400 × 400µm. Lower panels: *in vivo* appearance of the cornea inside and around the operated region. Top row: lamellar interfaces were marked by activated cells with increased reflectivity, with stellate-like morphology and cell processes visible (arrows). 2nd row: peripheral interfaces were marked by increased stromal cell reflectivity and formation of fibrous scar-type tissue (asterisks; im = BPC implant). 3rd row: in the central region of the surgical zone, stromal keratocytes in autografts appeared slightly activated with cell processes visible, while no cells were observed in BPCs. Bottom row: some stromal keratocytes in the peripheral surgical zone were activated in autografts (arrows), while a few stromal cells had migrated into the initially cell-free BPCs (arrows). All images 400 × 400µm.

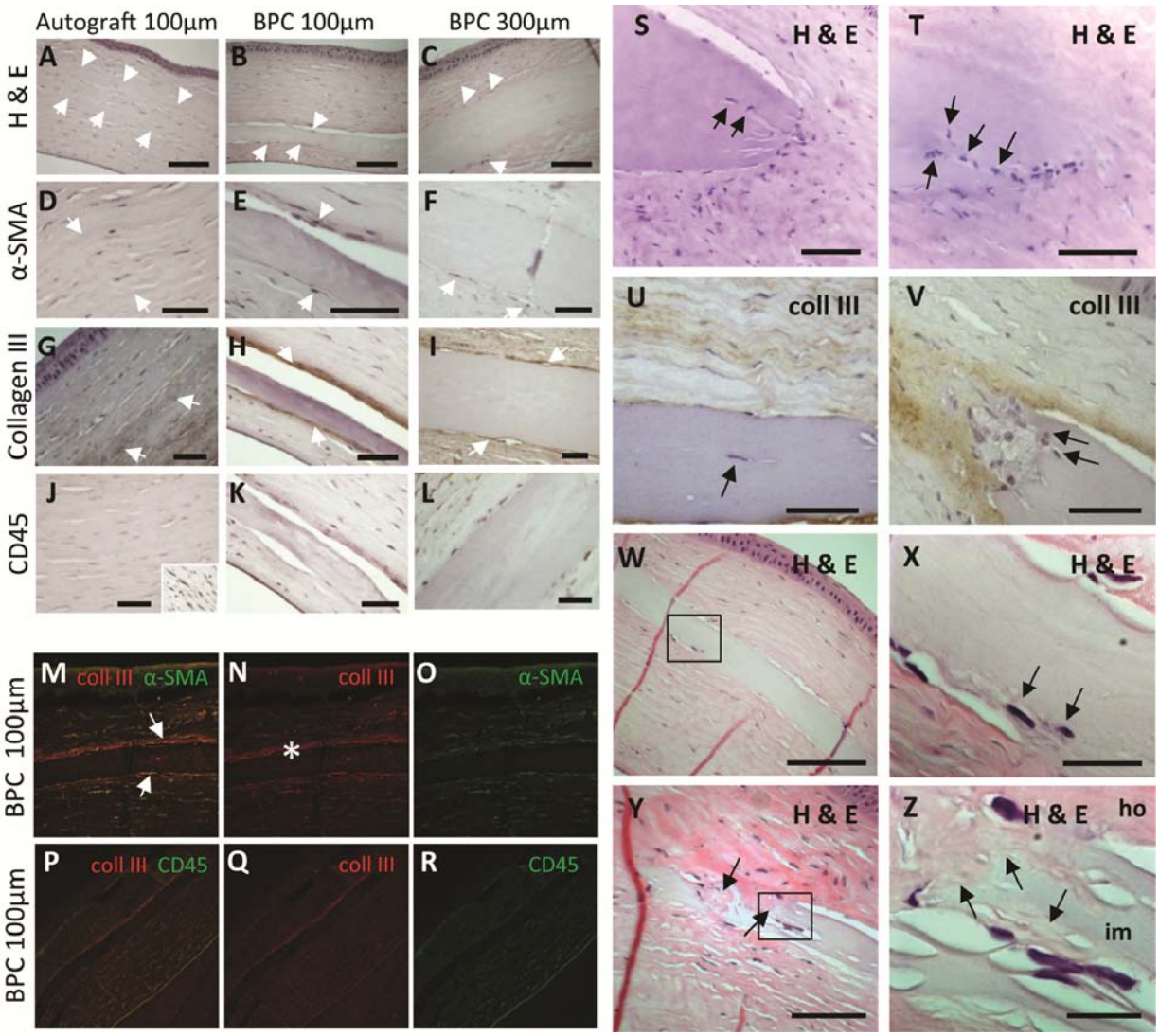

Fig. 5. Ex-vivo immunohistochemical analysis of BPCs indicates absence of inflammation, cell invasion, new collagen production, and turnover of implant into native collagen. (A) anterior and posterior laser cut regions were visible (arrows). (B, C) Stromal cells often lined biomaterial interfaces (arrows). (D) In autografts, interfaces (arrows) were not associated with α-SMA$^+$ myofibroblasts. (E, F) Myofibroblasts (arrows) lined the biomaterial interfaces. (G) A minimal production of type III collagen was noted around interfaces in atuograft tissue (arrows). (H, I) New type III collagen was produced at biomaterial-to-host lamellar interfaces (arrows). (J) No CD45$^+$ leukocytes invaded the surgical zone. Inset: positive control tissue with invading CD45$^+$ leukocytes consisting of a dense infiltrate of round and elongated cells. (K, L) Biomaterial implants were also free of leukocytic invasion. Scale bars: A-C: 100µm; D-L: 50µm. (M-R) Immunofluorescent staining revealed that α-SMA$^+$ myofibroblasts locate preferentially at implant-host interfaces and produce new type III collagen, without stimulating an inflammatory response. (M-O) Type III collagen is localized to host-implant interfaces and to individual α-SMA$^+$ stromal myofibroblasts (40× magnification). (P-R) CD45$^+$ leukocytes are absent from interfaces and the surrounding host stroma (20× magnification). (S-Z) Stromal cell migration and stromal regeneration in BPC implanted corneas

8 weeks postoperatively. (S, T) Cells appeared to migrate in single-file through apparent tunnels in the BPC (arrows). (U) Stromal cell deeper within a BPC (arrow), negative for type III collagen production. (V) Several stromal cells (arrows) migrating into the BPC edge, associated with type III collagen production and appearing to modify or degrade the BPC collagen. (W) Low-magnification view of the BPC with normal-appearing surrounding host tissue (Note: vertical red striations are artifacts). (X) Magnified view of boxed region in (W), indicating stromal cells invading the BPC (arrows), and modifying the collagen (color) of the BPC. (Y) The BPC is invaded by host stromal cells and BPC collagen is transformed to host collagen which exhibits a characteristic pink staining (arrows) Note: vertical red striations are artifacts. (Z) Magnified view of boxed region in (Y), indicating cell invasion of the implant and transformation of the grey-appearing BPC collagen (im) into pink-stained host collagen (ho, arrows). Scale bars S-V: 50µm; W,Y: 100µm; X,Z: 25µm.

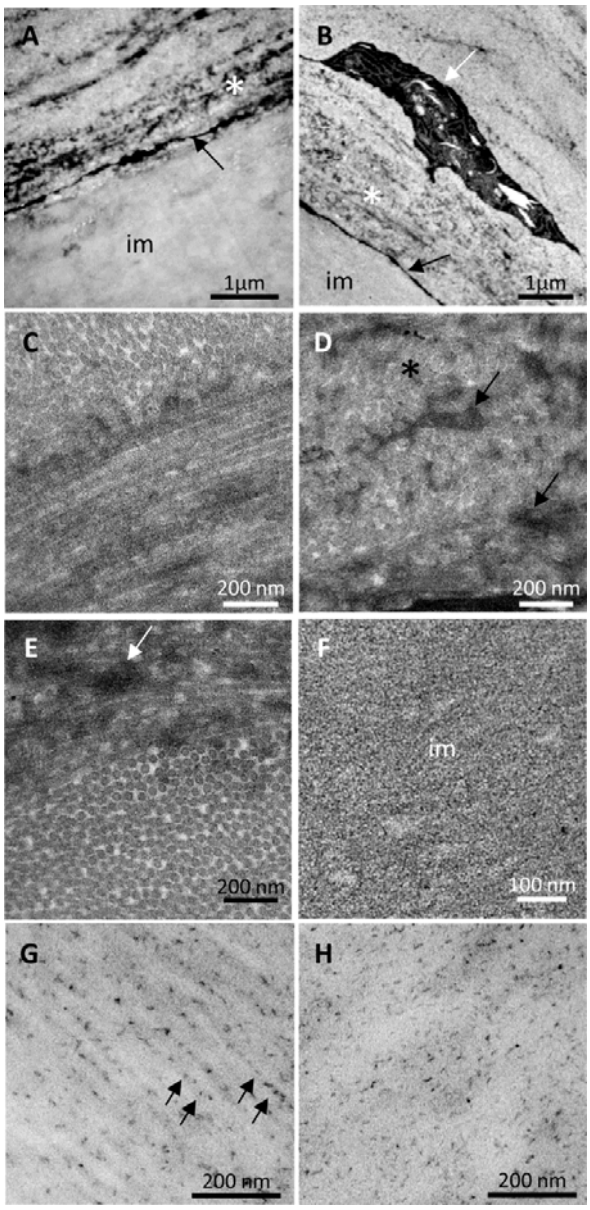

Fig. 6. Ex vivo transmission electron microscopy of 100µm thick BPC-implanted corneas 8 weeks postoperatively. (A) Anterior interface region, with remnant of the femtosecond laser cut visible (arrow). A band of modified collagen (asterisk) is present immediately anterior to the interface; im = BPC implant. (B) Stromal cells (white arrow) were observed close to the interface (black arrow) near the band of modified collagen (asterisk). (C) Higher magnification depicted the organized, lamellar structure of collagen fibrils in the host cornea. (D) High magnification view of the modified collagen band, which consisted of degraded/disrupted collagen fibrils (asterisk) and the presence of dark vacuoles (arrows). (E) Posterior interface transition zone of normal collagen lamellar structure to modified collagen structure, consisting of dark vacuoles (arrow) and discontinuous fibril organization. (F) High magnification image of the BPC implant reveals a lack of intact collagen fibrils or lamellar organization, and a granular, ultrafine structure. (G) In the host stroma, electron-dense

proteoglycans (arrows) were arranged linearly along the direction of collagen fibrils. (H) Proteoglycans were also present within the BPC, but were randomly distributed.

Supplementary File

Supplementary Video 1. Prior to the video, the femtosecond laser cuts have been made, but native tissue is still in place. In the video, the surgeon first removes the disc of native rabbit tissue from the central corneal stroma, via the arc-shaped access cut (Fig. 3*A*). The disc is 100µm thick. The surgeon then takes a pre-cut disc of 100µm thick BPC (the implant), and using surgical forceps, inserts this implant into the central corneal stroma using the same access cut.